

# 1 Introduction

Solar System history started some 4567 million years ago with the collapse of an interstellar molecular cloud to a protoplanetary disk (the solar nebula) surrounding a central star (the Sun). Evolution of the Solar System continued through a complex process of accretion, coagulation, agglomeration, melting, differentiation and solidification, followed by bombardment, collision, break-up, brecciation and re-formation, then to varying extents by heating, metamorphism, aqueous alteration and impact shock. One of the key goals of planetary science is to understand the primary materials from which the Solar System formed, and how they have been modified as the Solar System evolved. The last two decades have seen a greater understanding of the processes that led to the formation of the Sun and Solar System. Advances have resulted from astronomical observations of star-formation regions in molecular clouds, the recognition and observation of protoplanetary disks and planetary systems around other stars, and also from advances in laboratory instrumentation that have led to more precise measurements on specific components within meteorites, e.g., refinement of chronologies based on short-lived radionuclides. Results from meteorites are important because meteorites are the only physical materials available on Earth that give direct access to the dust from which the Solar System formed. Study of meteorites allows a more complete understanding of the processes experienced by the material that resulted in the Earth of today.

## 1.1 Naming of meteorites

Meteorites are pieces of rock and metal, almost all of which are fragments broken from asteroids during collisions. They fall at random over the Earth's surface, and have also been identified as components within lunar soils [1.1, 1.2] and on Mars' surface [1.3]. Meteorites are named from their place of find or fall, traditionally after a local geographic feature or centre of population. However, where large numbers of meteorites are found within a limited area, this convention is not possible to follow. The recovery of meteorites from desert regions has resulted in a name–number nomenclature that combines geographic and date information. Antarctic

specimens collected by government-funded expeditions are given a year–number combination with a prefix recording the icefield from which they were retrieved (e.g., Allan Hills 84001), whereas meteorites collected in hot deserts are simply numbered incrementally by region (e.g., Dar al Gani 262). The rules for naming newly recovered meteorites have been standardized by the Nomenclature Committee of the Meteoritical Society, which also assigns names to meteorites and keeps track of the total number of reported specimens. This information is available at <http://www.pi.usra.edu/meteor/metbull.php>.

Newly recovered meteorites are also reported in the *Meteoritical Bulletin* (published in the journal *Meteoritics and Planetary Sciences*, and updated regularly on the website as above). The *Catalogue of Meteorites*, last published in book form in 2000, is a database of all meteorites [1.4], and is also available through a searchable interface at <http://www.nhm.ac.uk/jdsml/research-curation/research/projects/metcat/>.

## 1.2 Classification of meteorites

Classifying meteorites enables similarities and differences between specimens to be recognized. This, in turn, allows inferences to be drawn about relationships between groups, their origins and the common processes that they have experienced. Over the years, meteorite classification has become a more precise science, partly as a result of the increasing sophistication of the instrumentation available for meteorite analysis, and partly owing to the increasing numbers of meteorites recovered from desert locations. Many schemes for classification have been devised, some with more utility than others, but all schemes, right from the very first descriptions of meteorites, recognized a basic division between stone and iron meteorites. Meteorites can be divided into two main types, according to the processes they have experienced: unmelted (unfractionated, undifferentiated) and melted (fractionated, differentiated). The unmelted meteorites, or chondrites, are all stones, and in all but the most volatile of elements, have compositions that are close to that of the solar photosphere. Melted meteorites

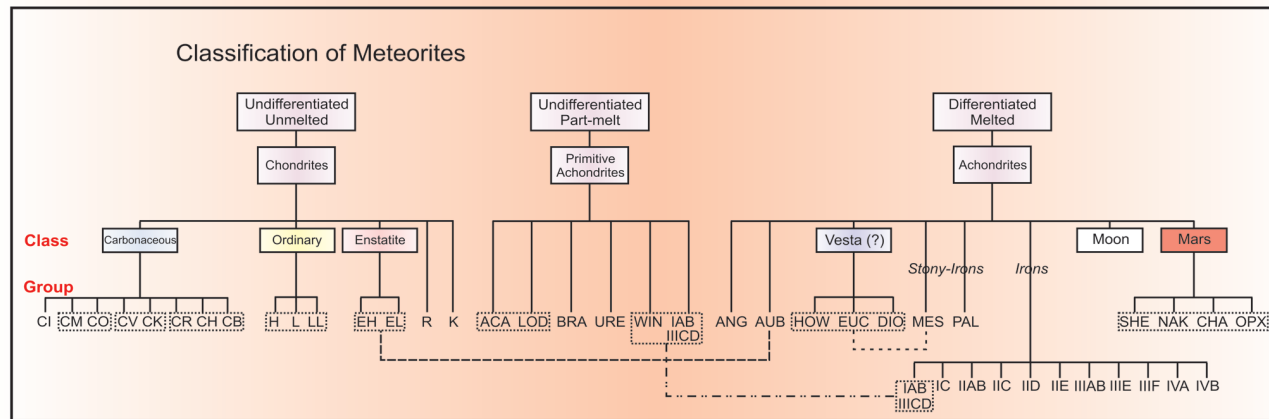


**Figure 1.1:** Schematic classification of meteorites, showing the main groups of each class. The dashed boxes and lines indicate clans (or supergroups) of meteorites that might have formed in closely neighbouring nebular or parent body locations [1.7]. ACA – Acapulcoites; ANG – Angrites; AUB – Aubrites; BRA – Brachinites; CHA – Chassignites; DIO – Diogenites; EUC – Eucrites; HOW – Howardites; LOD – Lodranites; MES – Mesosiderites; NAK – Nakhilites; OPX – Orthopyroxenite; PAL – Pallasites; SHE – Shergottites; URE – Ureilites; WIN – Winonaites. After [1.6, 1.7].

(achondrites) cover a range of compositions from stone, through stony-iron to iron. Bridging between these two major divisions are the primitive achondrites: meteorites that have an unfractionated composition, but textures that indicate they have been strongly heated, if not melted. Both unmelted and melted meteorites are further subdivided into classes and groups; their interrelationships are shown in the ‘family tree’ in Figure 1.1. Classification of meteorites is one way of identifying materials that might be associated in space and time, e.g., through accretion in closely neighbouring regions of the solar nebula, or having suffered similar processes of heating, melting, differentiation and/or hydrothermal alteration. Despite enormous progress brought about by increasing numbers of meteorites and advances in analytical instrumentation, the classification scheme is incomplete, and there are many meteorites that do not fit comfortably into the framework. There is not always a clear-cut distinction between types: e.g., there are many iron meteorites that contain silicate inclusions related to chondritic meteorites. Clasts and inclusions within meteorites also frequently defy ready assignment to recognized meteorite groups.

### 1.2.1 Historical background

One of the most detailed classification schemes was proposed in 1863 by the curator of the meteorite collection at the Mineralogical Museum in Berlin, Gustav Rose [1.5]. He subdivided meteorites according to their mineralogy, into three groups of iron meteorites (pure nickel–iron, pallasites

and mesosiderites) and seven groups of stones. It was Rose who first introduced the term *chondrule* (from the Greek *chondros*, meaning grain or seed) to describe the spherical globules present in many of the stony meteorites. He also named the chondrule-bearing meteorites *chondrites*, and recognized separate classes of *carbonaceous chondrites*, *eucrites*, *howardites* and *chassignites*, terms that all survive today.

Rose’s scheme was later expanded in 1883 by the custodian of the Vienna mineral and meteorite collection, Gustav Tschermak [1.8], who subdivided Rose’s iron meteorites into irons and stony-irons. Tschermak also attempted the first classification of iron meteorites on the basis of the width of the kamacite lamellae in the Widmanstätten pattern revealed by etching. Tschermak renamed Rose’s class of shalkites to *diogenites*. Tschermak’s successor at Vienna, Aristides Brezina, continued to modify and expand the classification system, to include divisions by structure and colour [1.9]. It was he who introduced the term *achondrite* to distinguish non-chondrule-bearing stones from chondrites. By the end of the nineteenth century, the combined Rose–Tschermak–Brezina system (RTB) of meteorite classification was the most widely used and accepted scheme throughout the international meteorite community. Although the RTB classification system, based on structure and mineralogy, was widely used, it was mostly a qualitative system, reliant on subjective judgements such as colour. Between 1916 and 1920, George T. Prior, Keeper of the Mineralogy Department at the (then) British Museum (Natural History)

proposed a revised and simplified meteorite classification scheme based on reliable chemical analyses [1.10, 1.11]. He formulated 'Prior's Rules', which noted the relationship between the amount of iron metal in a chondrite, and the iron content of its silicate: the less the amount of nickel-iron metal, the richer in iron are the silicates. The scheme subdivided the chondrites according to the iron content of their pyroxenes, into enstatite, olivine-bronzite and hypersthene-bronzite chondrites, and the achondrites into calcium-rich and calcium-poor groups. The Prior classification for chondrites is the basis of that in use today.

In 1953, Urey and Craig [1.12], using only what they termed 'superior' chemical analysis of chondrites, demonstrated that the chondrites were distinguishable on the basis of their total iron content, in addition to the extent of oxidation of this iron (Figure 1.2). The olivine-bronzite chondrites corresponded to a group which they termed H-group (for high total iron content, approximately 28%) and the hypersthene-bronzite chondrites to a group termed L-group (low total iron content, 22%). Prior [1.10, 1.11] had also noted that the hypersthene-bronzite chondrites could be further subdivided into two types, chemically and mineralogically distinct, the Baroti and Soko-Banja types. Mason and Wiik [1.13] found that the Soko-Banja-type meteorites were very similar to another, minor, group of meteorites, the amphoterites. Up until this time, analysis of mineral chemistry had relied on the painstaking separation of minerals from meteorites, followed by measurement using either wet chemistry or X-ray diffraction techniques. Keil and Fredriksson [1.14] were among the first analysts to apply the electron microprobe to meteorite samples, using thin sections of ordinary chondrites. They studied meteorites from Prior's Soko-Banja subgroup, and noted that they had the same total iron content as the L-group chondrites, but a lower iron metal (as opposed to oxidized iron in the silicates) content. On these grounds, the Soko-Banja-type meteorites and amphoterites were renamed the LL-group (for low total iron, low metallic iron). The three groups, H, L and LL chondrites, are now collectively known as **ordinary chondrites** (Chapter 3), and, without accounting for pairing, in total comprise some 87% of all known meteorites, around 95% of all chondrites [1.4].

The **carbonaceous chondrite** (Chapter 2) class of meteorites exhibits considerable variation in mineralogy. The term 'carbonaceous chondrite' is a misnomer on two counts: there are other meteorite groups (e.g., the ureilite achondrites, Chapter 9) that contain comparable amounts of carbon, and one of the carbonaceous chondrite groups (CI) does not contain chondrules. Notwithstanding this, the name has remained since Gustav Rose first introduced it in 1863. Carbonaceous chondrites may also be subdivided into chemically and

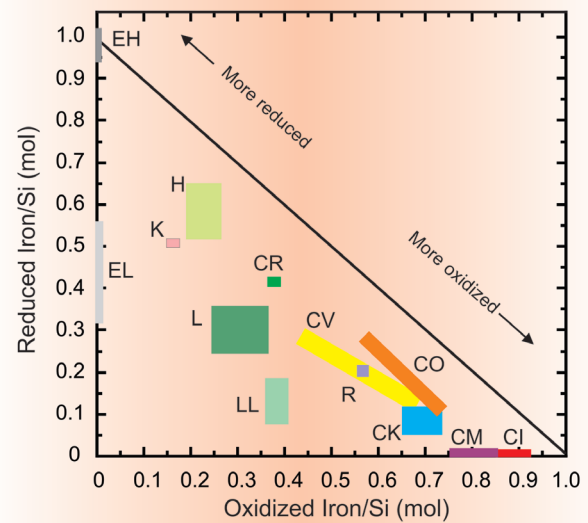


**Figure 1.2:** Urey–Craig plot, modified from [1.24], showing how the ratio of reduced iron (metal and sulphides) varies with oxidized iron (silicates and oxides) among the different chondrite groups. The line (slope  $-1$ ) is that along which meteorites with the same total iron content but different oxidation states would fall [1.24].

structurally distinct types. The first such distinction was made by Wiik [1.15], who based the divisions on volatile element content (C, H<sub>2</sub>O and S), as well as on the specific gravity of the meteorites. Using mean values of these criteria, he distinguished three types (I, II and III). Mason [1.16] redefined these types, following which they became the C1, C2 and C3 types according to mineralogy [1.17]. The C3 chondrites were further subdivided [1.18, 1.19] into the Ormans and Vigarano subtypes (C3(O) and C3(V), respectively).

The remaining class of chondrites, the **enstatite chondrites** (Chapter 4), named by Prior [1.10, 1.11] after their dominant mineral composition, show extreme variation in iron and sulphur contents [1.20]. These changes in composition also correlate with their degree of metamorphism [1.21, 1.22] and so the group was subdivided into two types [1.20]: EI (high iron and sulphur, little recrystallization) and EII (low iron and sulphur, highly recrystallized). The groups were renamed as EH and EL, respectively [1.23], by analogy with the high- and low-iron groups (H and L) of the ordinary chondrites.

Figure 1.2 is a modified version of the Urey–Craig plot (after ref. 1.24), showing the relative positions of the enstatite, carbonaceous and LL-group ordinary chondrites, in addition to the original H- and L-group ordinary chondrites. Other major element ratios (e.g., Mg, Ca and Al) have been used to separate the chondrites into various

**Table 1.1:** Criteria for assigning petrologic type to chondrites (after refs. 1.18, 1.24, 1.37)

Criterion	1	2	3	4	5	6
Homogeneity of olivine and low Ca-pyroxene	–	> 5% mean deviations		≤ 5%		Homogeneous
Structural state of low Ca-pyroxene	–	Predominantly monoclinic		> 20% monoclinic	< 20% monoclinic	Orthorhombic
Feldspar	–	Minor primary grains only		Secondary	Secondary	Secondary
Chondrule glass	–	Altered, mostly absent	Clear, isotropic, variable abundance	Devitriified, absent	< 2 μm grains	2–50 μm grains
Metal: maximum bulk Ni content		< 20%; taenite minor or absent	> 20%; kamacite and taenite in exsolution relationship			> 50 μm grains
Sulphides: mean Ni content	–	> 0.5 wt.%		< 0.5 wt.%		
Matrix	Fine-grained, opaque	Mostly fine, opaque	Clastic and minor opaque	Transparent, recrystallized,	coarsening from 4 to 6	
Chondrule–Matrix integration	No chondrules	Chondrules very sharply defined		Chondrules well defined	Chondrules readily delineated	Chondrules poorly defined
Carbon (wt.%)	3–5	0.8–2.6	0.2–1	< 0.2		
Water (wt.%)	18–22	2–16	0.3–3	< 1.5		

groups [1.17, 1.25–1.27]. Figure 1.3 illustrates these groups, distinguished by varying Ca/Si and Al/Si atomic ratios.

By the mid- to late-1960s, it had been recognized that not only were there variations in the chemistry and mineralogy of distinct meteorite groups, but there were very significant changes in texture that seemed to cut across the chemical differences. This led to a comprehensive chemical and petrological classification scheme for chondrites [1.18].

Mineralogical and structural criteria were used to define a two-dimensional grid (Table 1.1), into which fit both chemical and textural variations. This is the basis of the classification system used in meteorite work today. Van Schmus and Wood [1.18] recognized a variation in petrologic character among the ordinary chondrites, across a spectrum from unaltered (dis-equilibrium of iron in silicates, presence of glass, sharply defined chondrules) to altered (homogenous silicates, no glass, recrystallized matrix, containing only relict chondrules). This gradation of properties was numerated, to allow ready classification of ordinary chondrites, and is reproduced in Table 1.1.

Petrologic type was originally defined for, and applied to, ordinary chondrites. The definitions have subsequently been expanded and applied to all chondrite classes (Table 1.2). The increase in petrologic type of a meteorite, from type 3 to type 6, implies an increasing extent of thermal metamorphism, from practically unaltered (type 3) to metamorphosed and recrystallized (type 6). Petrologic types 3 to 6 are found in carbonaceous, ordinary and enstatite chondrites, whilst types 1 and 2 are confined to carbonaceous chondrites.

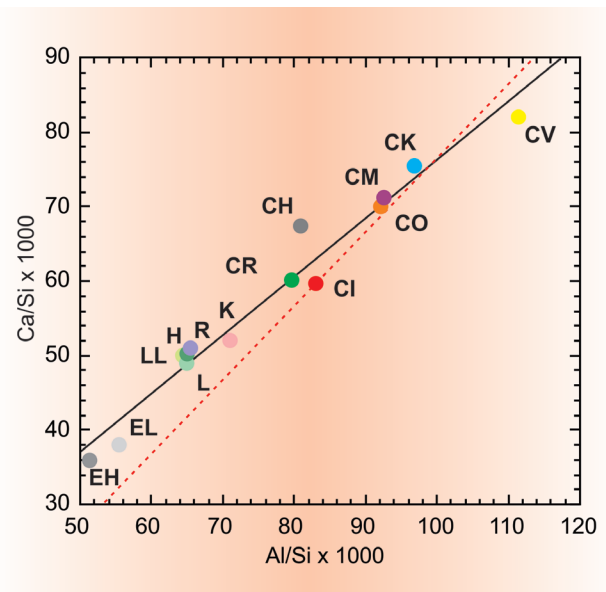


**Figure 1.3:** Plot of mean Ca/Si and Al/Si ratios for the different chondrite groups. The solid black line is the line of best fit to the data. The dashed red line is a line of slope 1 fit to the CI values. Data from [1.28–1.30].

Electron microprobe analysis of meteorites showed not only the very narrow range of olivine and pyroxene compositions exhibited by the H, L and LL groups of ordinary chondrites [1.14], but that mineralogy varies with petrologic

**Table 1.2:** Distribution of petrologic types by chondrite class

Total by number (June 2014)										Total by percentage (June 2014)									
1	2	3	4	5	6	7	Other*	Total		1	2	3	4	5	6	7	Other*	% by Group	
<b>Carbonaceous</b>										<b>Carbonaceous</b>									
CI	9	–	–	–	–	–	–	–	9	CI	100	–	–	–	–	–	–	–	0.5
CM	37	422	–	–	–	–	–	8	467	CM	7.9	90.4	–	–	–	–	–	1.7	27.2
CO	–	–	432	–	–	–	–	–	432	CO	–	–	100	–	–	–	–	–	25.2
CV	–	1	298	–	–	–	–	–	299	CV	–	0.3	99.7	–	–	–	–	–	17.4
CK	–	–	24	98	107	21	–	3	253	CK	–	–	9.5	38.7	42.3	8.3	–	1.2	14.7
CR	2	149	–	–	–	2	1	9	163	CR	1.2	91.4	–	–	–	1.2	0.6	5.5	9.5
CH	–	–	23	–	–	–	–	–	23	CH	–	–	100	–	–	–	–	–	1.3
CB	–	–	–	–	–	–	–	19	19	CB	–	–	–	–	–	–	–	100	1.1
Ungr <sup>§</sup>	2	16	17	6	1	2	–	8	52	Ungr <sup>§</sup>	3.8	30.8	32.7	11.5	1.9	3.8	–	15.4	3.0
Total	50	588	794	104	108	25	1	47	1717	% by Type	2.9	34.2	46.2	6.1	6.3	1.5	0.1	2.7	100
<b>Ordinary</b>										<b>Ordinary</b>									
H	–	–	900	5224	8079	4741	16	143	19103	H	–	–	4.7	27.3	42.3	24.8	0.1	0.7	44.8
H/L	–	–	17	18	7	12	–	–	54	H/L	–	–	31.5	33.3	13.0	22.2	–	–	0.1
L	–	–	912	1450	5261	8919	22	125	16689	L	–	–	5.5	8.7	31.5	53.4	0.1	0.7	39.1
L/LL	–	–	50	24	25	33	–	1	133	L/LL	–	–	37.6	18.0	18.8	24.8	–	0.8	0.3
LL	–	–	358	335	3038	2486	32	292	6541	LL	–	–	5.5	5.1	46.4	38.0	0.5	4.5	15.3
Ungr <sup>§</sup>	–	–	–	–	–	–	–	156	156	Ungr <sup>§</sup>	–	–	–	–	–	–	–	100	0.4
Total	–	–	2237	7051	16410	16191	70	717	42676	% by Type	–	–	5.2	16.5	38.5	37.9	0.2	1.7	100
<b>Enstatite</b>										<b>Enstatite</b>									
EH	–	–	122	27	6	7	2	8	172	EH	–	–	70.9	15.7	3.5	4.1	1.2	4.7	31.4
EL	–	–	20	14	7	81	1	3	126	EL	–	–	15.9	11.1	5.6	64.3	0.8	2.4	23.0
Ungr <sup>§</sup>	–	–	212	5	8	10	–	14	249	Ungr <sup>§</sup>	–	–	85.1	2.0	3.2	4.0	–	5.6	45.5
Total	–	–	354	46	21	98	3	25	547	%	–	–	64.7	8.4	3.8	16.8	0.5	4.6	100
<b>Rumurutiite</b>										<b>Rumurutiite</b>									
			66	49	24	10	–	3	152				43.4	32.2	15.8	6.6	–	2.0	100
<b>Kakangari-type</b>										<b>Kakangari-type</b>									
			2	–	–	–	–	1	3				66.7	–	–	–	–	33.3	100
<b>Ungrouped Chondrites</b>										<b>Ungrouped Chondrites</b>									
								15	15									100	100

For simplicity, anything labelled transitional (e.g., 3/4) or inclusive (e.g., 4–6), was binned into the lower type; this assumption has little effect on the overall percentages. More significantly, no account was taken of pairing, which does have a big effect on the absolute numbers of a category, but by and large not on the totals expressed by percentage. The table includes both falls and finds. If only meteorites that had been observed to fall were selected, pairing would not be an issue, but many of the more rare meteorite types would not show up (e.g., there would be no entry for CH chondrites, or for CK 5 and CK6).

\* The columns labelled ‘Other’ include impact melt breccias and unclassified meteorites; it also includes the CB meteorites, none of which has a designated petrologic type.

§ The rows labelled ‘Ungr’ include meteorites that have been assigned a petrologic type but not a chemical group. Data from the Meteoritical Bulletin website ([www.lpi.usra.edu/meteor/metbull.php](http://www.lpi.usra.edu/meteor/metbull.php); accessed June 2014).

grade [1.31, 1.32]. The dominant mineral phases present in all three ordinary chondrite chemical groups are olivine, pyroxene, feldspar, metal and sulphides. For the most part, in petrologic types 4–6, in all chemical groups, the olivines and low-calcium pyroxenes are homogenous with respect to

their iron contents, whereas in the type 3 chondrites, the iron content of the silicates is highly variable, more so in the pyroxenes than in the olivines [1.31]. The differences in silicate mineral composition led Dodd and Van Schmus [1.33] to coin the phrase ‘unequilibrated’ for those ordinary

chondrites in which the olivine and pyroxene iron content was inhomogeneous. The extent of this inhomogeneity also correlated with the degree of recrystallization of the mineral matrix. Hence type 3 ordinary chondrites are unequilibrated and higher petrologic types are equilibrated.

Up until the beginning of the 1970s, there was a slow but steady increase in the number of meteorites available for study, allowing progressive refinement of classification schemes. Meteorite taxonomy, however, suffered from a lack of specimens: frequently only unique examples of an apparent subdivision might be known, a problem that was particularly acute for the achondrites. The situation changed with the recovery of large numbers of meteorites from cold and hot deserts. In 1969, a team of Japanese glaciologists discovered nine meteorites in a restricted area of the Yamato Mountains in Antarctica [1.34]. The nine fragments were found to represent at least six different meteorites; subsequently, it has been recognized that vast numbers of meteorites accumulate in blue ice regions over the continent [1.35]. Since 1969, Antarctica has become the region from which the highest number of meteorites has been retrieved, over 35,000 by spring 2009. This is not because meteorites fall over Antarctica any more frequently than they do elsewhere over the globe, but a result of the unique mechanism that acts to preserve and concentrate meteorites in specific areas of the continent. The meteorites are also readily visible on the blue ice.

Hot deserts (e.g., the Sahara in Northern Africa and the Nullarbor Region of Western Australia), where the dry conditions prevent chemical degradation of metal, have also yielded several thousand meteorites [1.36]. The rapid increase in the numbers of meteorites available for analysis has led to developments in meteorite classification. There are now much greater numbers of ordinary chondrites, allowing subtle refinements of the petrological subclassification. But, perhaps more importantly, there are many more unusual and rare meteorites that have populated previously under-represented classes, extended the range of compositional variations shown by the major meteorite groups and expanded the number of recognized subdivisions. Over the last 30 years, meteorites from desert collections together with advances in scientific instrumentation have allowed revision and modification of the meteorite classification scheme that is now accepted and used internationally.

### 1.2.2 Chondrites

The increasing number of desert meteorites showed the limitations of the Van Schmus and Wood classification when

applied to type 3 ordinary chondrites: there is almost as much variation in chemical composition occurring in this class alone, as across the rest of the spectrum. The amount of unequilibration within the type 3 chondrites is also variable, some samples being recognizably more recrystallized than others. The need for further subdivision of the unequilibrated ordinary chondrites was recognized, and several workers proposed independent parameters for this division, including the distribution of cobalt in kamacite [1.38] and the extent of matrix recrystallization [1.39]. However, these parameters, based as they were on only a few measurements, distinguished only four subtypes. Sears and colleagues, using a much greater database, recognized 10 subtypes, distinguishable by their thermoluminescence (TL) sensitivity, which trended in the same manner as the parameters mentioned above [1.40]. The new groups were numbered from 0 to 9. Hence Semarkona, a highly unequilibrated ordinary chondrite, is classified as a type LL3.0, whereas Bremervörde, a more equilibrated type 3, is type H3.9. Classification into petrologic subtype is not linear, and is regarded as accurate to  $\pm 1$  subgroup [1.23, 1.40].

The Van Schmus and Wood classification system also required modification for application to carbonaceous chondrites. Their classification as C1, C2, C3(O) and C3(V) implied some type of genetic interrelationship, which was not necessarily the case. Wasson rechristened the groups CI, CM, CO and CV (corresponding to C1, C2, C3(O) and C3(V), respectively), the letters being the initials of the type specimens of each class: Ivuna, Mighei, Ornans and Vigarano [1.37]. A few years later, the CR class was added, after its type specimen, Renazzo [1.41].

Another significant advance in the history of meteorite classification was made in the late 1970s, by R. N. Clayton of the University of Chicago. Clayton measured the oxygen isotopic composition of silicates separated from individual meteorites, and found that different groups had different isotopic compositions [1.42–1.45]. Figure 1.4 shows the oxygen isotopic composition of the major chondrite groups. The variations in composition are generally taken to be a reflection of primordial nebular heterogeneity, modified in some groups as a result of widespread fluid–solid exchange processes.

It is two hundred years since the first paper was published on the chemical composition of meteorites [1.46]. We now recognize 15 different chondrite groups. There are eight carbonaceous chondrite groups: CI, CM, CO, CV, CR, CK [1.47], CB [1.48] and CH [1.49]. The type specimens for the CK and CB chondrites are Karoonda and Bencubbin, respectively. The CH chondrites are not named for a type specimen, but their relatively iron-rich composition is recognized with a

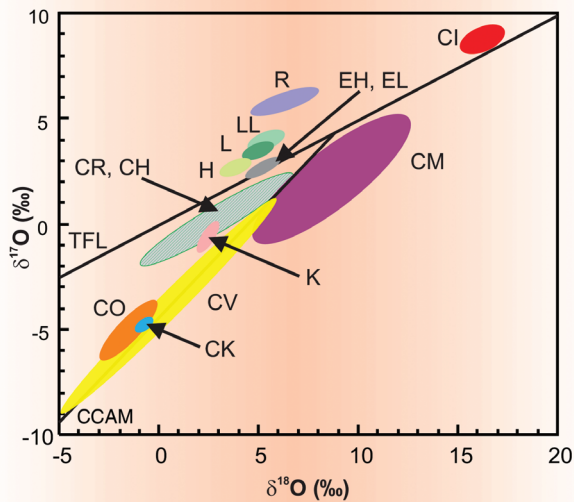


**Figure 1.4:** The oxygen isotopic composition of the different chondrite groups. TFL – Terrestrial Fractionation Line; CCAM – Carbonaceous Chondrite Anhydrous Mineral line. Data from [1.42–1.45] and references therein.

label analogous to that of the high-iron groups of the ordinary and enstatite chondrites [1.49]. As well as eight groups of carbonaceous chondrites, there are three groups of ordinary chondrites (H, L and LL), plus the EH and EL enstatite chondrites, and the rumurutiite (R) [1.50, 1.51] and Kakangari-type (K) chondrites [1.30] (treated together in Chapter 5). The groups are distinguished on the basis of elemental and isotopic chemistry, matrix, metal and chondrule contents and chondrule properties (size, type, etc.). The differences between the groups are primary, i.e., were established as the parent bodies accreted in different regions of the solar nebula. Subsequent to accretion, most meteorites have experienced varying extents of thermal metamorphism or aqueous alteration. These secondary processes occurred on the meteorites' parent bodies, and did not affect the overall composition of the chondrites. Mobilization and redistribution of elements such as Fe, Mg and Ca occurred as primary silicates either became homogeneous in composition through heating, or through formation of secondary mineral phases (e.g., clay minerals, carbonates) during aqueous alteration. The petrologic subclassification of chondrites, into H5, CM2, LL4, etc., is a reflection of secondary processes acting on a parent body, quantifying the extent of dry thermal or aqueous alteration experienced after the parent asteroid aggregated. The various meteorite classes have experienced secondary processes to different extents, demonstrated by variety in the

range of petrologic types exhibited by the groups (Table 1.2). It is also recognized that modification does not cease, even after metamorphism or metasomatism ends: collisions between asteroids lead to brecciation, and the production of shock veins and melt glass. These tertiary effects can be recognized as textural changes within mineral grains. There is a semi-quantitative scale for shock classification of ordinary chondrites [1.52] that has subsequently been applied to carbonaceous and enstatite chondrites [1.53, 1.54]. The scale is based on characterization of defects in silicate grains (mainly olivine), and ranges from S1 (unshocked) to S6 (highly shocked, to about 75–90 GPa) (Table 1.3).

The final parameter required to classify fully a chondrite is applied to meteorites that have been found, rather than those observed to fall, as it is a measure of the amount of weathering experienced by the meteorite during its terrestrial lifetime. Weathering rusts metal, and breaks down primary silicates to clay minerals; a semi-quantitative scale to assess the weathering grade of chondrites was proposed by Wlotzka [1.55]. Thus, a full classification of a shocked ordinary chondrite might be H5 (S4, W2). This designation gives an outline of the primary, secondary and tertiary pre-terrestrial history of the rock, as well as an indication of its terrestrial history. The texture of a chondrite results from a combination of two factors: its constituents (i.e., the relative abundances of different components, including matrix, chondrules, metal, etc.) and the processes that the chondrite (or its parent body) has experienced (thermal metamorphism, fluid alteration).

### 1.2.3 Primitive achondrites

The distinction between chondrites and achondrites is no longer as clear as was the case when Mason [1.56] described five separate achondrite groups on the basis of their calcium content [1.56]. Four groups (the **acapulcoite–lodranite** clan (Chapter 6), **brachinites** (Chapter 7), **winonaites** (Chapter 8) and **ureilites** (Chapter 9); type specimens Acapulco, Lodran, Brachina, Winona and Novo Urei, respectively) are regarded as primitive achondrites (Figure 1.1). They have almost chondritic compositions (i.e., they are very little fractionated relative to the Sun), but their textures indicate that they have experienced some degree of heating and partial melting. Winonaites are closely related to the silicate inclusions in IAB irons, and may derive from the same parent body, bridging between iron meteorites and chondrites. The characteristics of primitive achondrites may help in the understanding of early differentiation processes in asteroidal bodies. Figure 1.5 shows the oxygen isotopic compositions of the primitive achondrite groups.

**Table 1.3:** Shock classification of meteorites [1.52–1.54]

Shock stage	Effects resulting from equilibration peak shock pressure				Shock pressure (GPa)
	Olivine	Orthopyroxene	Plagioclase	Local effects	
S1 Unshocked	Sharp optical extinction; irregular fractures			None	< 4–5
S2 Very weakly shocked	Undulose extinction; irregular fractures			None	5–10
S3 Weakly shocked	Planar fractures; undulose extinction; irregular fractures	Clinoenstatite lamellae on {100}; undulose extinction; planar fractures; irregular fractures	Undulose extinction	Opaque shock veins; incipient formation of melt pockets, sometimes interconnected	15–20
S4 Moderately shocked	Weak mosaicism; planar fractures	Weak mosaicism; twinning on {100}; planar fractures	Undulose extinction; partially isotropic; planar deformation features	Melt pockets; interconnecting melt veins; opaque shock veins	30–35
S5 Strongly shocked	Strong mosaicism; planar fractures and planar deformation features	Strong mosaicism; planar fractures	Maskelynite	Pervasive formation of melt pockets, veins and dikes; opaque shock veins	45–55
S6 Very strongly shocked	Restricted to local regions in or near melt zones			As for S5	75–90
Shock melted	Solid state recrystallization and staining; ringwoodite; melting Whole rock melting (impact melt rock and melt breccias)	Majorite; melting	Shock melted (normal glass)		

### 1.2.4 Achondrites

Achondrites are meteorites that formed from melts, and thus have differentiated compositions. Achondrites traditionally only comprised stony meteorites that had lost a large fraction of their primordial metal content, their name emanating from the observation that such meteorites generally do not contain chondrules. However, the current convention is to regard all differentiated meteorites (stone, iron and stony-iron) as achondrites (Figure 1.1).

#### 1.2.4.1 Asteroidal stone achondrites

Stony achondrites differ from chondrites in their major element content, especially calcium and similar elements. They have almost no metal or sulphides, and neither do

they contain chondrules. They are mainly composed of crystals that appear to have grown from a melt. There are many different groups of achondrites, some of which can be linked together to form associations allied with specific parents. The separate associations have little, if any, genetic relationship to each other. Figure 1.5 shows the oxygen isotopic compositions of the different achondrite groups.

**Angrites** (Chapter 10; type specimen Angra dos Reis) are medium- to coarse-grained basaltic igneous rocks. Although the angrites have similar oxygen isotopic compositions to the HEDs (Figure 1.5), they are unrelated. **Aubrites** (or enstatite achondrites (Chapter 11), type specimen Aubres) are highly reduced meteorites with mineralogies and oxygen isotopic compositions similar to those of enstatite chondrites, leading to the suggestion that aubrites might have formed by partial melting of an enstatite chondrite precursor.

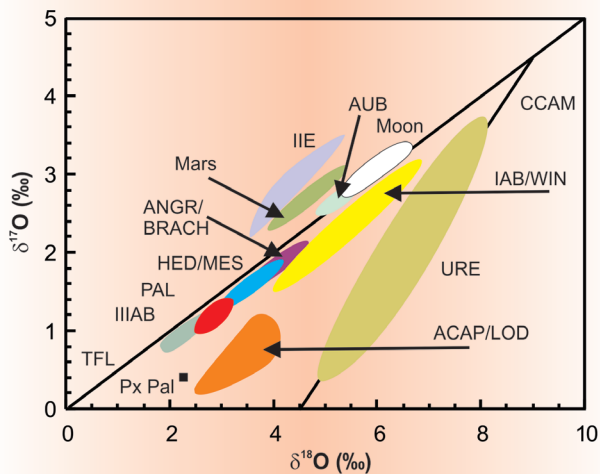


**Figure 1.5:** The oxygen isotopic composition of different achondrite groups. TFL – Terrestrial Fractionation Line; CCAM – Carbonaceous Chondrite Anhydrous Mineral line. Data from [1.41, 1.45].

The **howardite–eucrite–diogenite** (HED) clan (Chapter 12) is a suite of generally brecciated igneous rocks ranging from coarse-grained orthopyroxenites (**diogenites**) to cumulates and fine-grained basalts (**eucrites**). The **howardites** are regolith breccias, rich in both solar wind gases and clasts of carbonaceous material. The HEDs all have similar oxygen isotopic compositions (Figure 1.5); a strong candidate for the HED parent body is asteroid 4 Vesta.

### 1.2.4.2 Stony-irons

The stony-irons are divided into two groups: **mesosiderites** (Chapter 13) and **pallasites** (Chapter 14), similar only in their approximately equal proportions of silicate and metal. The two groups have very different origins and histories. Mesosiderites are a much more heterogeneous class of meteorites than the pallasites. They are a mixture of varying amounts of iron–nickel metal with differentiated silicates, the whole assemblage of which seems to have been brecciated (Figure 1.6).

**Pallasites** are perhaps the most strikingly beautiful of all meteorites. They are an approximately equal mixture of iron–nickel metal and silicates (predominantly olivine), and the metal forms a continuous network, into which the olivine grains are set (Figure 1.7). Pallasites are presumed to represent material from the core–mantle boundary of their parent bodies.

### 1.2.4.3 Iron meteorites

Iron meteorites (Chapter 15) are highly differentiated materials, presumed to be products of extensive melting processes on their parents. They are composed of iron metal, generally with 5–15 wt.% nickel, and account for approximately 5% of all observed meteorite falls. The mineralogy of iron meteorites is dominantly an intergrowth of two phases, the iron–nickel metals kamacite and taenite. Kamacite, or  $\alpha$ -Fe-Ni, has a body-centred cubic structure and a Ni content

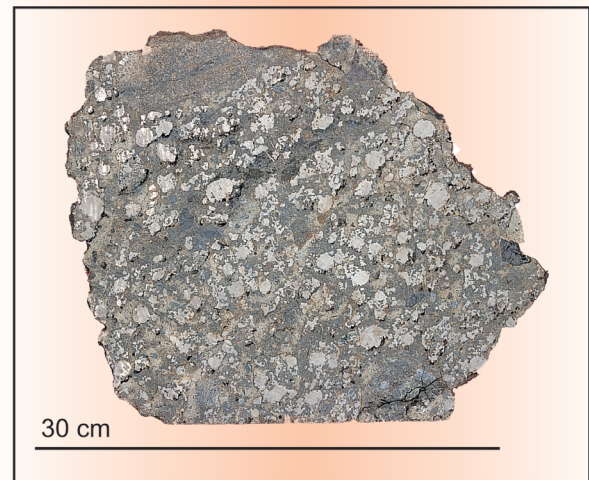


**Figure 1.6:** A cut slice from the Estherville mesosiderite, showing a range of different clast types.

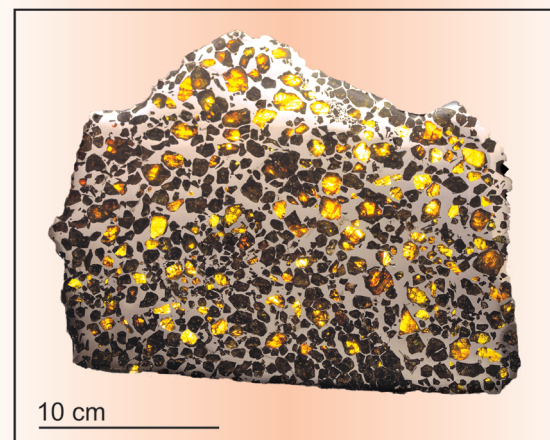


**Figure 1.7:** A cut and polished slice of the Esquel pallasite. The slice is sufficiently thin that the olivine grains appear transparent.

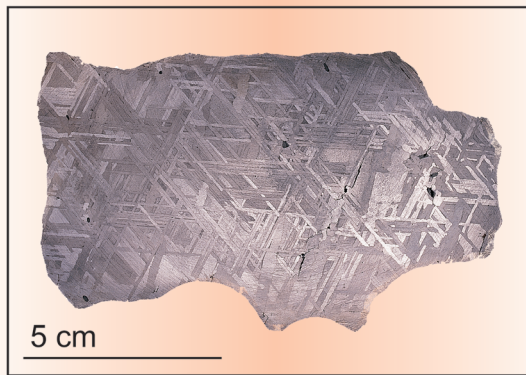


**Figure 1.8:** A polished and etched slab of the Henbury iron meteorite, illustrating the Widmanstätten pattern.

< 7 wt.%, whilst taenite, or  $\gamma$ -Fe-Ni, is face-centred cubic and approximately 15–50 wt.% Ni. When polished and etched in dilute mineral acid, irons reveal a distinctive structure, known as a Widmanstätten pattern (Figure 1.8). This consists of plates of kamacite in an octahedral orientation with interstices between the platelets filled with taenite and plessite (a very fine-grained, submicron, intergrowth of kamacite and taenite). The width of the kamacite lamellae is related to the cooling history of the parent bodies. The pattern is named for Aloys J. B. von Widmanstätten, who, at the start of the nineteenth century, observed the pattern on several iron meteorites, although he probably was not the first to describe the structure [1.57].

The coarseness of the Widmanstätten pattern is expressed as the width of the kamacite lamellae (or bandwidth), and iron meteorites were originally classified by Tschermak [1.8] into five structural groups: the coarse, medium and fine octahedrites, ataxites and hexahedrites. The structural classification of iron meteorites was redefined and made systematic by V.F. Buchwald [1.58].

Structural classification of iron meteorites has been succeeded by classification based on metal composition [1.59]. The irons are subdivided into 12 different groups on the basis of nickel and trace element chemistries (Ga, Ge and Ir contents); see Figure 15.2. The relatively tight coupling between Ni and Ga and Ge for 10 of the individual groups (Figure 1.1) indicates that the groups represent discrete parents that had completely melted and then solidified by fractional crystallization [1.59]. These groups were previously known as the magmatic iron meteorites, although this term is no longer in favour [1.6].

Two groups, the IAB and IIICD irons, have a wide range in Ga and Ge abundance with Ni content. They were thought to derive from parent bodies that had not completely melted, and were coupled together as non-magmatic iron meteorites that possibly formed during impact processes on their parent asteroids. It is now recognized that silicate inclusions in the IABs are very closely linked to the winonaite group of primitive achondrites. Winonaites and IABs, if not coming from the same parent body, must at least have formed in closely located regions of the solar nebula [1.60, 1.61].

Many irons defy chemical classification, and simply remain ungrouped. The chemical classification of iron meteorites has mainly been undertaken by J.T. Wasson and coworkers at UCLA. On the basis of trace-element compositions, it is estimated that iron meteorites might represent samples of at least 70 individual asteroids.

#### 1.2.4.4 Non-asteroidal stone achondrites

All the meteorites that have been considered so far originated from asteroids. In the early 1980s, it was recognized that there were two groups of meteorites derived from planetary rather than asteroidal sources. **Lunar meteorites** (Chapter 16) are mostly anorthositic regolith breccias. The lunar origin of the meteorites is certain: the mineralogy and chemistry of the samples is indistinguishable from that of the samples returned directly by the Apollo astronauts. **Martian meteorites** (Chapter 17) almost certainly originate on Mars. There have been many missions to Mars since the first successful fly-by of Mariner 4 in 1965. Imagery and other data from orbiting satellites and landed craft have increased our knowledge of Mars and our understanding of its formation, the relative chronology of the major events that shaped its surface, and the mineralogy of the surface materials. A valuable source of information about Mars, complementary with data returned from space missions, is the class of meteorites that were ejected from Mars' surface by impact. Although we do not (yet) have rocks returned directly from Mars by spacecraft with which these rocks can be compared, the Martian origin of the meteorites is fairly secure, and is based on the age, composition and noble gas inventory of the meteorites.

### 1.3 Components of chondrites

Chondrites are mechanical mixtures of a variety of components that originated at different times in different regions of the protosolar nebula. They also contain, to a greater or lesser extent, grains that originated prior to the formation of the solar nebula (presolar grains). The relative abundances and sizes of

the major chondritic components are essential indicators of the classification of a meteorite. The mineralogy of chondritic constituents is described briefly here, and expanded in the relevant chapter introductions. There have also been several papers reviewing meteorite mineralogy, the most comprehensive of which is by Brearley and Jones [1.24].

### 1.3.1 Refractory inclusions

There are several varieties of refractory inclusion (RI), but the most studied are the calcium- and aluminium-rich inclusions (CAI), amoeboid olivine aggregates (AOA) and FUN inclusions (Fractionated and Unknown Nuclear effects). Of these, CAI are the most abundant, and the terms refractory inclusion and CAI are often used interchangeably. For detailed descriptions of the properties of RI see the reviews by Brearley and Jones [1.24] and MacPherson [1.62]. Calcium- and aluminium-rich inclusions (CAI) are irregularly shaped objects within many chondrites of petrologic types 2–3 (Figure 1.9). As their name implies, they are composed of calcium- and aluminium-rich minerals, such as hibonite, melilite, spinel, etc., as well as fassaite, an aluminium-bearing pyroxene. These minerals are characterized by their refractory nature; their presence implies that CAI formed in high-temperature processes (temperatures  $>1800$  K), probably in a region very close to the newly formed Sun. The mineralogy and isotopic composition of CAI identified them as objects that formed very early on in the history of the Solar System. Discussions of CAI formation have previously assumed that they were produced by direct condensation from the cooling nebular gas [1.63]. Whilst this is presumably correct for some CAI, others have textures that suggest formation from partially molten droplets [1.64]. CAI are currently regarded as aggregates of primary nebular condensates that may have experienced several episodes of partial melting and alteration in the nebula prior to accretion into parent bodies; secondary alteration also occurred during subsequent parent-body evolution [1.62]. Age-dating of minerals within CAI has shown that they are the oldest objects in the Solar System, with ages of 4567 Ma [1.65]. Following their formation (which seems to have occurred on a time-scale of  $<1$  Myr), CAI were transported to the regions in which chondrite parent bodies were aggregating.

Because (i) CAI in CV3 chondrites are large in size (up to  $\sim 2.5$  cm across) and abundant in distribution (up to 10 vol.%) (see Table 2.1) and (ii) the Allende CV3 chondrite shows the full spread of CAI varieties and is itself widely distributed and in abundant supply, CAI in CV3 have been extensively studied. As a consequence, most of the information we have about CAI is based on the study of CV3

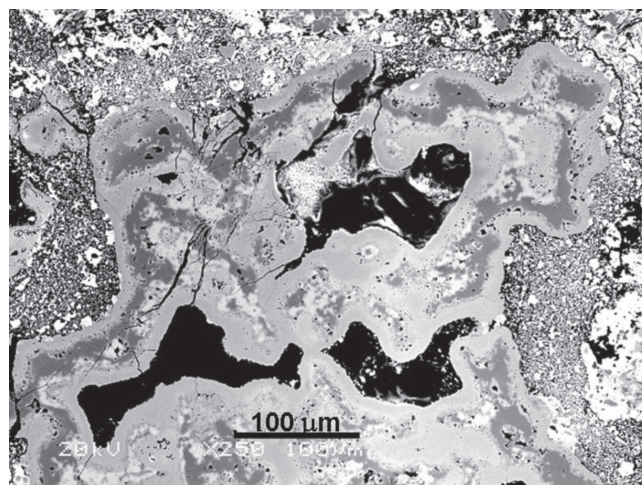


**Figure 1.9:** Scanning electron microscope (SEM) image of part of a fluffy type A CAI from the Ormans CO3 chondrite.

chondrites in general, and Allende in particular. CAI are often surrounded by a layered sequence of rims, composed of spinel, perovskite, hibonite, melilite and pyroxene (Figure 1.9). Each layer is usually composed of only one or two mineral species. The rims follow the outline of a CAI closely, even fractured where the CAI is fractured, so it was assumed that the rims were of nebular rather than parent-body origin [1.66].

CAI are subclassified on the basis of texture into coarse-grained ( $>10$   $\mu\text{m}$ ) and fine-grained inclusions (Figure 1.10). The former are subdivided on the basis of mineralogy into types A, B and C (Figure 1.11) [1.68]. Type A CAI are the most abundant and widespread; they occur in all groups of carbonaceous chondrites, as well as ordinary, enstatite and rumurutiite chondrites. They are large, up to  $\sim 2$  cm in size, and are subdivided into fluffy and compact objects [1.69]. Fluffy type A (FTA) CAI are made up of melilite, spinel, perovskite and pyroxene, with subordinate hibonite. Although the outline of the inclusion might be fluffy, mineral chemistry implies that FTA CAI have been annealed following recrystallization. Compact type A CAI are more granular than FTA, and are composed of relatively coarse-grained tabular melilite plus spinel, hibonite, perovskite and pyroxene.

Type B CAI have only been identified in CV chondrites. They are large, up to 2.5 cm across, mainly pyroxene plus anorthite and spinel, with lesser amounts of melilite [1.64]. Type C CAI are mostly rounded droplets rich in anorthite. Their texture suggests solidification from a melt [1.68]. Fine-grained CAI are mainly spinel-rich inclusions  $<1$  cm across composed of grains  $<20$   $\mu\text{m}$  in size [1.64, 1.70]. The most abundant phase is spinel, accompanied by other minerals including hibonite, anorthite, fassaite, feldspathoids

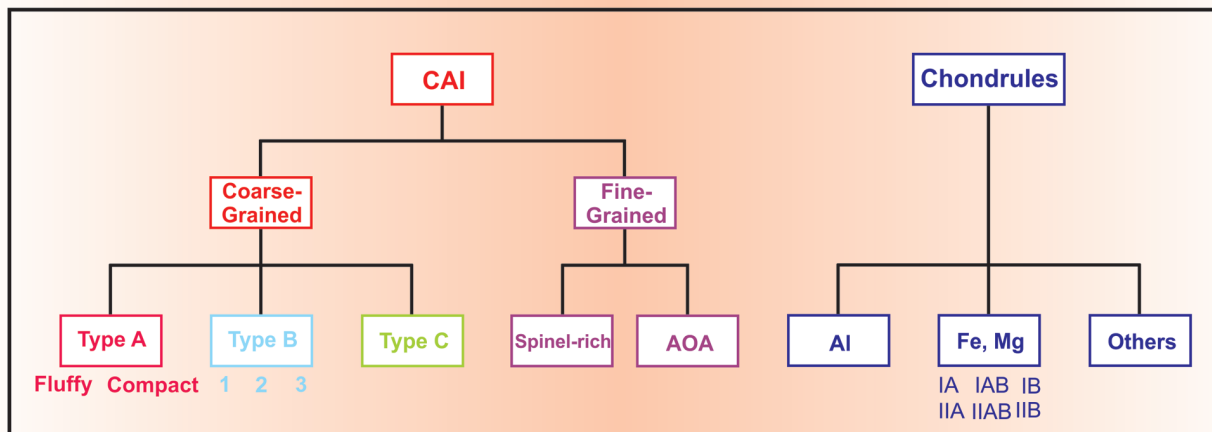


**Figure 1.10:** Subclassification of CAI and relationship with chondrules. After [1.67].

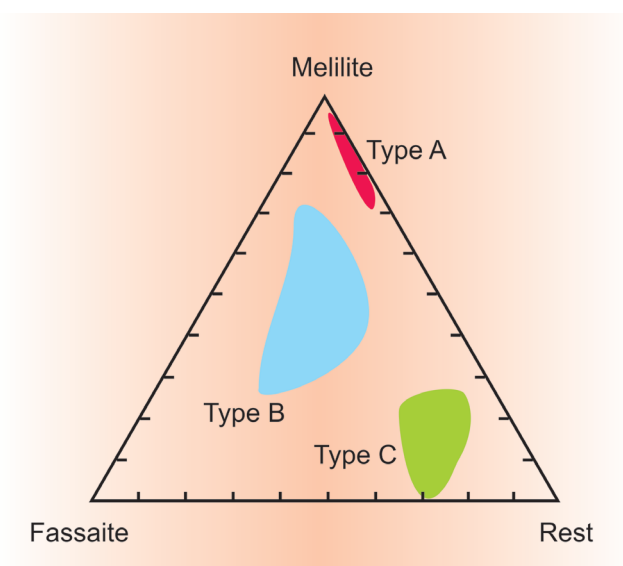


**Figure 1.11:** Classification of coarse-grained CAI. The end-member ‘Rest’ includes all components other than melilite and fassaite. After [1.24, 1.68].

(nepheline, sodalite) and olivine [1.24]. The inclusions are often rimmed by Wark–Lovering rims [1.71].

Amoeboid olivine aggregates (AOA) are often included in descriptions of CAI, although in terms of mineral chemistry, they are not particularly Ca- or Al-rich [1.72]. They are fine-grained, up to a centimeter in size, composed of forsteritic olivine (<20 μm) plus spinel, pyroxene, feldspathoids and sulphides [1.64]. There has been speculation that AOA and

aluminium-rich chondrules form a bridge between CAI and chondrules [1.73–1.75].

A third group of refractory inclusions is a subset of CAI known as FUN inclusions, for Fractionation and Unidentified Nuclear effects – properties that these particular inclusions display [1.76]. FUN inclusions are indistinguishable from other CAI in terms of their mineralogy and mineral chemistry. They have clearly had a different history from other CAI, because although they do not have the excess in  $^{26}\text{Mg}$  (from decay of  $^{26}\text{Al}$ ) exhibited by CAI, they do show large fractionations (the F in FUN) in Mg and O isotopes, as well as anomalous isotopic compositions in a variety of other elements, including Ca, Ti, Cr and Ba (the UN in FUN) [1.77]. It is not clear what relationship FUN inclusions have with the main CAI population.

### 1.3.2 Chondrules

The origin of chondrules is a matter of vigorous and active debate within the meteoritical community. Their spherical to subspherical shape and internal texture indicate that they formed in a high-temperature process, and that they are quenched droplets of once-molten silicates (Figure 1.12). Both the location of chondrule formation, and the process that rendered solid grains of interstellar dust molten, are uncertain: Boss [1.78] catalogued nine different processes that might have been responsible for chondrule formation, giving reasons for and against each process. More recently, two main formation mechanisms have been favoured: in the

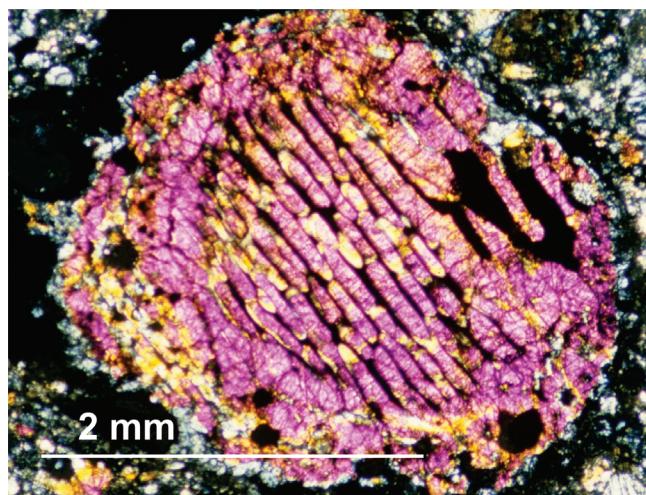


**Figure 1.12:** A barred olivine (BO) chondrule from the Palmyra L3 ordinary chondrite.

**Table 1.4:** Chondrule textures [1.82]

Type	Mineralogy	Origin
PO	Porphyritic olivine	Solidified from partially molten droplets
PP	Porphyritic pyroxene	
POP	Porphyritic olivine and pyroxene	
BO	Barred olivine	Solidified from fully molten droplets
RP	Radial pyroxene	
C	Cryptocrystalline	

outflow from the young Sun (the X-wind model [1.79]) or in shock waves [1.80]. It is possible that more than one mechanism was involved in chondrule formation, and that chondrules were produced by different processes at different locations within the nebula at different times [1.81].

Schemes for the classification of chondrules have evolved over many years, with contributions from many authors. Chondrules are described in terms of texture (Table 1.4) [1.82], and then subclassified on the basis of composition [1.83]. Type I chondrules are reduced, FeO-poor objects with mg# of olivine and pyroxene  $>90$ , whilst type II chondrules are more oxidized, richer in FeO, and have mg#  $< 90$  [1.24]. Additional information on the mineral constituents of chondrules is given by division into A or B, where group A chondrules contain phenocrysts of olivine, and group B, phenocrysts of pyroxene [1.84]. Differences in chondrule size, mineralogy, mineral chemistry and texture help to define the different chondrites classes and groups.

Chondrules from several different chondritic groups have been dated, giving ages in the range 4562–4567 Gyr [1.65, 1.85]. The most ancient age for chondrules has an uncertainty that overlaps with the apparent age of CAI (Figure 1.14 below). For many years, it seemed that the formation of CAI and chondrules were separated in time by about 3 Ma [1.75]. It now appears that CAI and chondrules began forming at almost the same time, but that chondrule formation continued for about 3 million years after CAI formation (Figure 1.14) [1.65].

### 1.3.3 Matrix

The matrix of a chondrite is its groundmass, the material that occurs between chondrules and other discrete objects (including chondrule fragments, CAI and CAI fragments, isolated large silicate, metal and sulphide grains) [1.86]. The matrix is fine-grained (micron to submicron) and mainly composed of silicates, although phyllosilicates and organic material are present in low petrologic type chondrites. Matrix abundance in the different chondrites groups is variable, from CI chondrites that are, in effect, 100% matrix, to enstatite chondrites with very little matrix at all. As well as forming the groundmass between chondrules, matrix also occurs as rims around chondrules and as individual lumps. As indicated in Table 1.1, the texture of matrix, its degree of recrystallization and the extent to which matrix can be distinguished from chondrules are all parameters employed in assignment of petrologic type to a chondritic specimen.

### 1.3.4 Presolar grains

A volumetrically insignificant, but scientifically critical component within chondrites is their complement of submicron- to micron-sized interstellar and circumstellar grains. These materials, which include silicon carbide, graphite and diamond, as well as silicates and oxides, are present at levels of a few ppb to ppm and have a variety of origins that pre-date formation of CAI and chondrules [1.87]. The grains are characterized and classified according to the isotopic composition of their major elements, and the noble gases that are trapped within them. Presolar grain abundance decreases rapidly with petrologic type, and the material is more or less absent from chondrites with petrologic type higher than about 3.6. In consequence, most studies have been made on presolar grains from CI and CM meteorites, where grain abundance is highest. Only the three most abundant types of presolar grain are described here (diamond, silicon carbide and graphite). For information on the full range of presolar

species, the reader is referred to review papers by Ernst Zinner and his colleagues [1.88–1.91].

Nanodiamonds are the most abundant presolar grains found in meteorites, and were the first to be isolated [1.92]. They are present in concentrations of up to ~1500 ppm in CI1 and CM2 chondrites [1.93, 1.94]. Unfortunately, however, their small size (~2–3 nm across) precludes measurement of individual crystallites, and as a result, analyses are of populations of grains, perhaps causing differing compositions of several nanodiamond components to be averaged out [1.95]. The nanodiamonds have a  $\delta^{13}\text{C} \sim -30\%$  to  $-35\%$  and  $\delta^{15}\text{N} < -340\%$  [1.94] and, relative to  $^{130}\text{Xe}$ , contain xenon enriched in  $^{124}\text{Xe}$ ,  $^{126}\text{Xe}$ ,  $^{134}\text{Xe}$  and  $^{136}\text{Xe}$  isotopes compared with  $^{128}\text{Xe}$ ,  $^{129}\text{Xe}$ ,  $^{131}\text{Xe}$  and  $^{132}\text{Xe}$ . This xenon isotopic composition, enriched as it is in heavy and light isotopes, is known as Xe-HL, and its production mechanism is only poorly understood. It is inferred to have been produced in a supernova, and its nanodiamond carrier presumed to have formed by chemical vapour deposition in the expanding shell of the supernova [1.96, 1.97]. Attempts to separate nanodiamonds into different populations on the basis of grain size and density have identified a distinct component with  $\delta^{13}\text{C}$  up to  $+200\%$  and  $\delta^{15}\text{N} < -500\%$  that might originate in an AGB star [1.95]. Calculations show that only approximately 1 in  $10^6$  of the nanodiamonds contain Xe-HL [1.98]; the majority of the nanodiamonds must have a different source. It has been suggested, given the relatively restricted carbon and nitrogen isotopic compositions (close to solar), that not all nanodiamonds are presolar, and may have formed during collisions within the protoplanetary disk [1.98, 1.99].

Presolar silicon carbide accounts for up to around 15 ppm of CI1 and CM2 carbonaceous chondrites. Most SiC grains (~90% of the total, known as mainstream SiC) are a single population [1.89, 1.100]. They have  $\delta^{13}\text{C} \sim -100\%$  to  $+10,000\%$  and  $\delta^{15}\text{N} \sim 980\%$  to  $+2000\%$ , and, relative to  $^{130}\text{Xe}$ , contain xenon enriched in  $^{128}\text{Xe}$  and  $^{132}\text{Xe}$  isotopes compared with  $^{129}\text{Xe}$  and  $^{131}\text{Xe}$ . This xenon isotopic composition is characteristic of s-process xenon, and mainstream SiC grains are thought to be synthesized in an environment where s-process nucleosynthesis dominates, such as in low-mass AGB stars [1.101]. There are additional, less abundant SiC grain populations that may emanate from J- and R-type carbon stars and ejecta from type II supernovae [1.89, 1.90, 1.100, 1.102]. These grains are characterized by  $\delta^{13}\text{C} \sim -960\%$  to  $+60,000\%$  and  $\delta^{15}\text{N} \sim 980\%$  to  $+26,000\%$  [1.103].

Presolar graphite comprises up to ~10 ppm of CM2 chondrites [1.89] and exhibits a range of crystallinities (and thus densities) [1.104]. The graphite grains have  $\delta^{13}\text{C} \sim -970\%$

to  $+30,000\%$  and  $\delta^{15}\text{N} \sim 0\%$  to  $+8000\%$ . Some of the grains carry neon produced by the decay of the short-lived radioisotope,  $^{22}\text{Ne}$ , and must have been produced in a supernova [1.91]. Other possible sources for graphite include novae [1.105], He-burning in Wolf–Rayet stars or type II supernovae [1.89, 1.106] or ion–molecule reactions in molecular clouds [1.107].

## 1.4 Noble gases

All meteorites contain noble gases, as mixtures of components with different origins. The components can be subdivided into two categories: (i) those that are carried by isotopically unusual grains that are inferred to be of presolar origin and (ii) those that are associated with the solar nebula within which their parent objects aggregated. Noble gas components in category (i), trapped or implanted within presolar grains, are present only in chondritic meteorites of low petrologic type, and were described in Section 1.3.4. Noble gas components in category (ii) have four separate origins: cosmogenic, radiogenic, solar and planetary. Cosmogenic noble gases occur in all meteorites, produced by the interaction of galactic (and solar) cosmic rays with the meteorites during exposure in space. Discussion of cosmogenic noble gases and their employment as chronometers is described in Section 1.5.3. Similarly, radiogenic noble gases occur in many meteorites, produced as daughter isotopes from the decay of radioactive parents. Discussion of radiogenic noble gases and their employment as chronometers is described in Section 1.5.4.

Solar noble gases are implanted from the solar wind to a depth of a few microns into materials exposed on the surface of their parent body. Thus, surface regolith breccias of all chondrite classes, as well as several achondrite groups, contain solar noble gases. The component is characterized by a composition dominated by  $^4\text{He}$  and  $^{20}\text{Ne}$  relative to the heavier noble gases, reflecting the abundance of the different gases in the solar wind (Figure 1.13). Note, though, that the solar component implanted in meteorites may be fractionated with respect to the Sun, partly because of differential implantation efficiencies, and partly because the different species are accelerated to different extents within the solar wind [1.108, 1.109].

The planetary noble gas component in meteorites has an elemental pattern in which the heavier noble gases are present in higher abundance than the lighter, i.e., the opposite pattern to the solar elemental abundance pattern (Figure 1.13). The component is known as ‘planetary’ because the elemental pattern is similar to that of the terrestrial and Martian atmospheres [1.112]; a label such as

**Table 1.5:** Radiometric age-dating chronometers. Data from [1.117, 1.118]

Short-lived			Long-lived		
Parent	Daughter	Half-life (Myr)	Parent	Daughter	Half-life (Gyr)
$^7\text{Be}$	$^7\text{Li}$	53.1 days	$^{190}\text{Pt}$	$^{186}\text{Os}$	489
$^{41}\text{Ca}$	$^{41}\text{K}$	0.102	$^{147}\text{Sm}$	$^{143}\text{Nd}$	106
$^{36}\text{Cl}$	$^{36}\text{S}, ^{36}\text{Ar}$	0.301	$^{87}\text{Rb}$	$^{87}\text{Sr}$	48.8
$^{26}\text{Al}$	$^{26}\text{Mg}$	0.717	$^{187}\text{Re}$	$^{187}\text{Os}$	41.6
$^{60}\text{Fe}$	$^{60}\text{Ni}$	1.5	$^{176}\text{Lu}$	$^{176}\text{Hf}$	35.7
$^{10}\text{Be}$	$^{10}\text{B}$	1.51	$^{232}\text{Th}$	$^{208}\text{Pb}, ^4\text{He}^{\S}$	14.01
$^{53}\text{Mn}$	$^{53}\text{Cr}$	3.74	$^{238}\text{U}$	$^{206}\text{Pb}, ^4\text{He}^{\S}$	4.45
$^{107}\text{Pd}$	$^{107}\text{Ag}$	6.5	$^{40}\text{K}$	$^{40}\text{Ar}$	1.27
$^{182}\text{Hf}$	$^{182}\text{W}$	8.90	$^{235}\text{U}$	$^{207}\text{Pb}, ^4\text{He}^{\S}$	0.70
$^{205}\text{Pb}$	$^{205}\text{Tl}$	17.3			
$^{129}\text{I}$	$^{129}\text{Xe}$	15.7			
$^{92}\text{Nb}$	$^{92}\text{Zr}$	34.7			
$^{244}\text{Pu}$	$\text{Xe}, \text{Kr}^{\dagger}$	80.0			
$^{146}\text{Sm}$	$^{142}\text{Nd}$	103			

$^{\S}$   $^4\text{He}$  produced during decay can be used to determine the gas retention age of a specimen.

$^{\dagger}$  Decays by spontaneous fission, producing tracks within mineral grains

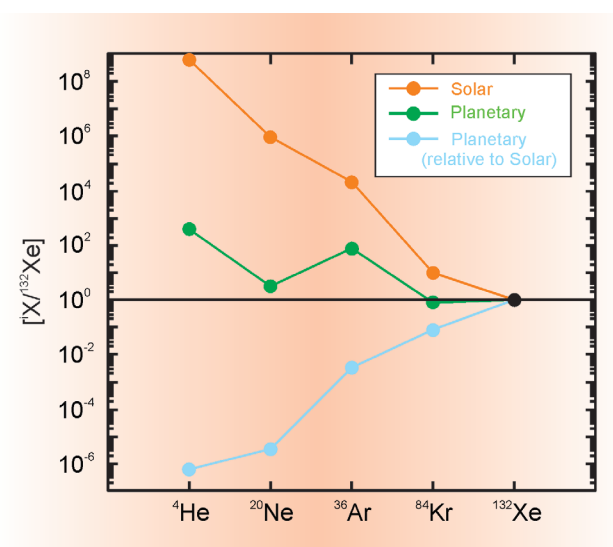


**Figure 1.13:** Abundances of solar and planetary noble gases relative to  $^{132}\text{Xe}$ . Solar abundance data are from the Genesis capture mission [1.110]; planetary abundance data are taken from [1.111] and are the average of results from carbonaceous and ordinary chondrites. The remaining curve plots the planetary data from [1.111] relative to the Genesis data [1.110], to give the more familiar curve illustrating the dominance of heavy over light noble gases in the planetary component known as Q or P1.

‘garbage-can’ [1.108] is probably closer to reality, since the component is what is left once solar, cosmogenic, radiogenic and presolar components are subtracted from a specimen’s noble gas inventory [1.108]. The planetary component is

also known as P1, and as Q; its origin is unknown (although it is assumed to be of local, Solar System provenance), as is its host or carrier phase [1.112]. Planetary noble gases are most abundant in chondrites of low petrologic type; exceptions to this are (i) the ureilites, which contain a component that appears to be closely related to planetary gases in chondrites [1.113, 1.114] and (ii) Martian meteorites, which contain trapped Martian atmosphere [1.115].

## 1.5 Age-dating of meteorites

The main events that led to the formation and evolution of the Solar System (CAI and chondrule formation, aggregation, crustal melting, differentiation and core formation) can be followed by several different radiometric age-dating chronometers (Table 1.5). An underlying assumption of the dating technique is that the parent isotope was distributed homogeneously through the meteorite (asteroid) formation regions, which seems to be the case [1.116].

The principle behind radioactive isotope dating is the fixed rate with which an unstable radioactive isotope (the parent) decays to a stable isotope (its daughter). The time taken for a radionuclide to decay to half its initial abundance is the half-life ( $t_{1/2}$ ) of the system. Several isotope systems with different half-lives are used to measure different events within Solar System history (Table 1.5). In practice, absolute abundances are not measured; rather, the isotopes are normalized to the amount of a related stable isotope, and isotope ratios measured. The absolute age of a sample is obtained

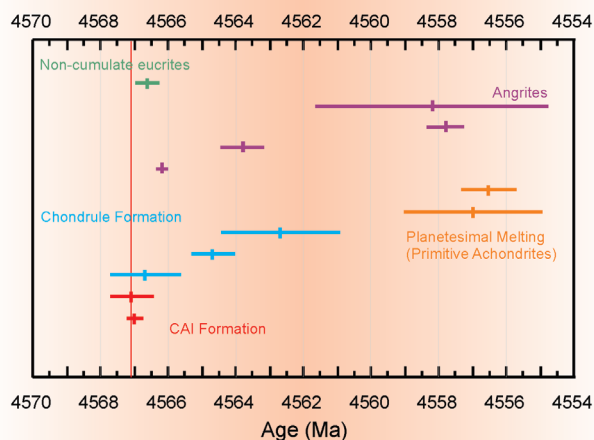


**Figure 1.14:** Time-scale of events taking place in the first 15 million years of Solar System history, based on Pb–Pb ages. Data from [1.65, 1.85, 1.117, 1.121 and references therein].

using the U–Pb system. The two separate isotopes of uranium ( $^{235}\text{U}$  and  $^{238}\text{U}$ ) decay at different rates to two different isotopes of lead ( $^{207}\text{Pb}$  and  $^{206}\text{Pb}$ , respectively; see Table 1.5). The ratio of the two daughter isotopes,  $^{207}\text{Pb}/^{206}\text{Pb}$ , can be measured very precisely, and if several components from a single sample can be measured, the resulting isochron yields an age. The Pb–Pb age obtained in this way is an absolute age. Short-lived radioisotope systems provide ages that are relative to the Pb–Pb absolute age; if a sample that has a Pb–Pb age is also dated by a short-lived chronometer, then the two ages can be compared directly and the time-scales inter-calibrated. Absolute ages have now been determined for many meteorite classes and meteoritic components (Figure 1.14).

### 1.5.1 Formation age

The oldest components in meteorites are the CAI, with ages (determined by U–Pb dating) of  $4567 \pm 0.1$  Myr [1.65]. This age can be taken as a baseline from which the date of formation of other meteoritic components can be measured. The decay of the short-lived radionuclide  $^{26}\text{Al}$  has been applied extensively as a fine-scale chronometer for determination of the relative ages of early Solar System events [1.117 and references therein]. Because Al and Mg are both lithophile elements, they are insensitive to metal–silicate fractionation processes, and so the  $^{26}\text{Al}$ – $^{26}\text{Mg}$  chronometer is used to constrain the formation time-scale of primitive rocky materials. This has led to the establishment of a relative time-scale for the production of CAI and chondrules. The ‘canonical’

model for accretion rationalized that the short-lived radionuclides were produced externally to the presolar nebula (probably in a supernova), injected into the collapsing dust cloud and incorporated into the CAI, etc., on time-scales shorter than that of the radionuclide half-life. For example, the presence of  $^{26}\text{Mg}$  within CAI shows that the CAI formed whilst  $^{26}\text{Al}$  was still ‘live’ in the solar nebula, i.e., agglomeration took place over a very short time-scale,  $<1$  Myr [1.119]. The  $^{41}\text{Ca}$ – $^{41}\text{K}$  chronometer implies even more rapid formation of CAI, with an interval between nucleosynthesis and agglomeration of  $<0.3$  Myr [1.120]. The most abundant component within chondrites, *viz.* chondrules, show little evidence for live  $^{26}\text{Al}$ ; measurements on aluminium-rich chondrules using the Al–Mg chronometer imply that chondrules formed after CAI production, and that chondrule formation took place over an extended period of time, commencing very shortly after CAI formation, and completing within  $<5$  Myr [1.85, 1.121, 1.122]. This is compatible with the Pb–Pb ages of chondrules, which imply that the onset of chondrule formation was almost simultaneous with CAI formation, but which then continued for several million years after CAI formation was completed (Figure 1.14) [1.65].

### 1.5.2 Planetary melting and differentiation

Following planetsimal accretion, silicate melting occurred, the heat source for which was presumably radioactive isotope decay combined with impact-induced heating. Subsequent crystallization results in partitioning of elements between different mineralogical components; a suitable radioisotope chronometer for measuring the age of crystallization of a melt (i.e., the time when elemental exchange could no longer occur between phases) is one where parent and daughter isotopes have different cosmochemical behaviours, such that, for example, the parent partitions into one silicate mineral (e.g., olivine), whilst the stable isotope of the daughter element moves into a second mineral, e.g., pyroxene. One such radiometric chronometer is the  $^{53}\text{Mn}$ – $^{53}\text{Cr}$  system ( $t_{1/2} = 3.74$  Myr), which has been extensively employed to date the timing of crystallization of early-formed igneous rocks, such as angrites [1.123]. Concordance between the Mn–Cr and Pb–Pb isotope systems in angrites has been used to pin the two chronometers together, allowing absolute age differences to be inferred on the basis of measurements of short-lived radioisotope decay products [1.117, 1.124].

The final stage in the gross evolution of a planetary embryo is melting of large volumes of material, leading to metal–silicate differentiation, segregation of metal and core

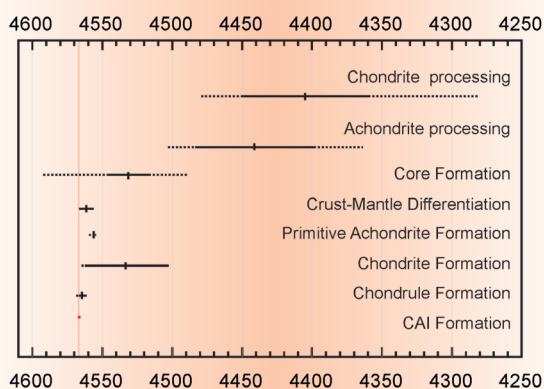


**Figure 1.15:** Time-scale of events taking place in the first 200 million years of Solar System history, based on several different chronometers and anchored to Pb–Pb ages. Data from [1.65, 1.85, 1.117, 1.121, 1.124–1.126 and references therein].

formation. Again, these processes can be followed by application of a suitable chronometer, for example the hafnium–tungsten system ( $^{182}\text{Hf}$ – $^{182}\text{W}$ ;  $t_{1/2} \sim 9$  Myr), which has been used to date metal–silicate differentiation on the Earth, Moon, Mars, and asteroidal parents [1.117]. Both hafnium and tungsten are highly refractory elements that are present in approximately chondritic relative abundances in bulk planets and planetesimals. However, during metal–silicate differentiation (or core formation), the lithophile Hf segregates into the silicate fraction whilst the siderophile W segregates into the metallic core. If this differentiation event occurs within  $\sim 5$  half-lives of  $^{182}\text{Hf}$ ,  $\sim 45$  Myr, then its timing can be determined by measuring the excess of the daughter product,  $^{182}\text{W}$  [1.124]. This has enabled new estimates for the timing of metal–silicate differentiation on the terrestrial planets and planetesimals (Figure 1.15). Iron meteorites started to form only  $\sim 1$  Ma after CAI formation [1.125, 1.126]. The onset of core formation is now thought to have occurred within the first  $\sim 3$  [1.127],  $\sim 13$  [1.128],  $\sim 10$ – $29$  [1.127], and  $\sim 29$  [1.127] Myr from the beginning of Solar System formation for Vesta, Mars, Earth and the Moon, respectively. These time-scales are significantly shorter than those determined previously for each of these planetary bodies [1.129–1.131].

### 1.5.3 Cosmic-ray exposure age

Cosmic-ray exposure (CRE) age is the length of time material has been exposed to cosmic radiation, whether on the surface of its parent, or whilst travelling as a body through space. Recent reviews [1.109, 1.132] give full descriptions

of how CRE ages are calculated. High-energy galactic cosmic-rays (GCR) penetrate to a depths of a few tens of centimetres [1.133], and so material buried at depth on a parent body is not exposed until impact excavates it to the surface. GCR induce nuclear reactions within exposed material, resulting in production of secondary species (cosmogenic nuclides). The cosmogenic nuclide produced is dependent on the composition of the target material:  $^{21}\text{Ne}$  from  $^{23}\text{Na}$ ,  $^{24}\text{Mg}$ ,  $^{27}\text{Al}$  and  $^{28}\text{Si}$ ;  $^{38}\text{Ar}$  from  $^{39}\text{K}$ ,  $^{40}\text{Ca}$ ,  $^{56}\text{Fe}$ , etc. For the major rock-forming elements (excluding oxygen), the most abundant secondary species produced are noble gases. There have been many measurements of the production rates of different cosmogenic nuclides [1.134]; production rates relevant for specific meteorite compositions have also been calculated [1.135]. The CRE age of a specimen is a simple relationship between abundance of a secondary nuclide, its production rate, and the concentration of the primary species in the meteorite. The foregoing description assumes that the body has only experienced a single stage of cosmic irradiation. Materials with more complex irradiation histories, e.g., break-up and re-irradiation of a body in space, require more detailed modelling to determine CRE age history [1.132].

Solar cosmic-rays (SCR) resulting from solar flares also generate secondary nuclides through spallation, but at a much lower rate than production by GCR. SCR have a different energy spectrum from GCR, and so have a shallower penetration depth. It is usually found that SCR-produced secondary nuclides are lost during atmospheric entry heating, and so do not contribute to CRE age calculations [1.109].

There are some broad generalizations that can be made for the CRE ages of meteorites, summarized by [1.132]. The CRE ages of iron meteorites are often  $>200$  Myr, whereas those of stony meteorites are mostly  $<100$  Myr and those of stony-irons are intermediate between the two values. The reason for the relationship between meteorite category and CRE age is presumably because the iron meteorites, being much more durable, are able to survive a higher number of collisions in space than the less indurated stony meteorites, and therefore have longer lifetimes.

### 1.5.4 Thermal and shock histories

The thermal and shock histories of meteorites are illustrated by changes in mineralogy and texture. The time when such changes occurred can be determined from measurement of the noble gas inventory of a specimen, because these species are mobile, and readily lost during secondary processing. As long as a system remains undisturbed (i.e., not shocked or

metamorphosed), the abundance of noble gases that have accumulated in a specimen is a record of how much time has elapsed since its final disturbance. This gas retention age might be dating the crystallization of a rock from a melt, or the era when thermal metamorphism occurred, or the timing of a shock event such as catastrophic break-up of a parent object [1.136]. The noble gas species most significant for determination of thermal or shock history is  $^{40}\text{Ar}$  (from  $\beta$ -decay of  $^{40}\text{K}$ ), yielding a  $^{40}\text{K}$ - $^{40}\text{Ar}$  age, which is the age of closure to argon, either since crystallization (in an undisturbed sample), or since the last thermal or shock event in a disturbed sample. An equivalent age is obtained by a variant on the technique, whereby neutron irradiation of a specimen converts  $^{39}\text{K}$  into  $^{39}\text{Ar}$ , giving an  $^{40}\text{Ar}$ - $^{39}\text{Ar}$  age. Measurement of  $^{40}\text{Ar}$ - $^{39}\text{Ar}$  ages of lunar samples and meteorites have shown clusters in ages that are related to impact and break-up events [1.136].

## 1.6 Genesis of chondrites

The genesis of different chondrite classes and groups is discussed in the relevant chapters. Here, however, we make a few general points about chondrite genesis. Both CAI and chondrules exhibit a range of sizes; it used to be thought that where large CAI occurred in a group, then large chondrules were also present and that the same relationship applied for small CAI and chondrules, implying that a size-sorting mechanism must have been in operation prior to aggregation of material into parent bodies [1.137, 1.138]. However, it now appears that the relationship between CAI and chondrule size no longer holds [1.139]. Even so, there are dynamic difficulties that must be addressed before a coherent model for chondrite formation can be produced. The age difference of up to  $\sim 4$  Ma between CAI and chondrules (Figure 1.14) is sufficient to have resulted in significant compositional differences between the two sets of components. On such a time-scale, the (presumably) mm- to cm-sized CAI would have spiralled into the newly formed Sun, and been destroyed; how CAI could be maintained in a discrete reservoir for up to 4 Ma is not well understood [1.139].

## 1.7 Genesis of achondrites

Given that CAI are the oldest objects in the Solar System, it has been assumed that chondrites were older than achondrites. However, with the advent of instrumentation able to measure increasingly low concentrations of trace elements, it has become possible to determine very precisely the relative ages of achondrite groups. It has become clear

from Pb-Pb dating of meteorites that the episodes of melting that led to formation of achondrites occurred very early in Solar System history, within 1 Ma from CAI formation (Figure 1.14). This would seem to be logical, assuming that heat from the decay of radionuclides was the main heat source for melting. So it is now accepted that there is temporal overlap between the formation of chondrites and achondrites (Figure 1.15), and that the evolution of the Solar System was not a simple chronological progression from chondrites to achondrites, but that heterogeneities within the presolar nebula might account for the synchronous formation of chondrites and achondrites.

## 1.8 Summary

It is not the purpose of the *Atlas of Meteorites* to provide an exhaustive review or description of components within meteorites; rather, we focus on specific features that will aid in recognition and classification of meteorites. Thus we have attempted to adopt a common format for each chapter in the *Atlas*. There is an introductory text to each chapter to give context to the images and thin-section descriptions. This text comprises a brief introduction to the class in question, including the current (as of June 2014) number of specimens and an outline of any system of subclassification. This is followed by a description of the main mineral components, the texture of the samples and their chemistry (major, minor, trace and rare earth element abundances) as well as oxygen isotopic composition. Noble gas and radiogenic isotope data are then discussed under age-dating studies. The final section of the introductory text is a summary of current theories on the genesis of each meteorite class, and a review of potential parent asteroids. Each chapter has a self-contained bibliography; references within the meteorite descriptions are also listed there. The main body of each chapter consists of meteorite descriptions accompanied by images. The recovery information is drawn, with slight modification, from the *Catalogue of Meteorites* [1.4]. The petrologic descriptions are of the specific meteorite specimens that were photographed, unless indicated otherwise. There are generally three images taken for each meteorite: under plane-polarized transmitted light, between cross-polarized transmitted light and under plane-polarized reflected light. Additional images (including meteorite specimens not included in the printed atlas) are on the CD that accompanies the book. The meteorite images can be freely used (for non-profit purposes), but please acknowledge the *Atlas* in any publications.

## REFERENCES

- [1.1] Anders E. et al. (1973). *The Moon* 8, 3–24;
- [1.2] McSween H.Y. Jr. (1976). *EPSL* 31, 193–199;
- [1.3] Schröder C. et al. (2008). *J. Geophys. Res.* 113, E06S22;
- [1.4] Grady M.M. (2000). *The Catalogue of Meteorites*. Cambridge Univ. Press. 689 pp;
- [1.5] Rose G. (1863). *Abhandl. Akad. Wizz. Phys.-Math. Kl. Berlin*. 166 pp;
- [1.6] Weisberg M.K. et al. (2006). In: *Meteorites and the Early Solar System II* (eds. D. Lauretta & H.Y. McSween), Univ. Arizona Press, Tucson, Arizona, 19–52;
- [1.7] Krot A.N. et al. (2007). In: *Meteorites, Comets, and Planets* (ed. A.M. Davis), Vol. 1 *Treatise on Geochemistry* (eds. H.D. Holland & K.K. Turekian), Elsevier-Pergamon, Oxford, Ch. 1.05, 83–128;
- [1.8] Tschermak G. (1883). *Sitzber. Akad. Wiss. Wien, Math-Naturw.* 8, 347–371;
- [1.9] Brezina A. (1904). *Proc. Am. Phil. Soc.* 43, 211–247;
- [1.10] Prior G.R. (1916). *Min. Mag.* 18, 26–44;
- [1.11] Prior G.R. (1920). *Min. Mag.* 19, 51–63;
- [1.12] Urey H.C. & Craig H. (1953). *GCA* 4, 36–82;
- [1.13] Mason B. & Wiik H.B. (1964). *GCA* 28, 533–538;
- [1.14] Keil K. & Fredriksson K. (1964). *J. Geophys. Res.* 69, 3487–3515;
- [1.15] Wiik H.B. (1956). *GCA* 9, 279–289;
- [1.16] Mason B. (1963). *Sp. Sci. Rev.* 1, 621–646;
- [1.17] Van Schmus W.R. & Hayes J.M. (1974). *GCA* 38, 47–64;
- [1.18] Van Schmus W.R. & Wood J.A. (1967). *GCA* 31, 747–765;
- [1.19] Van Schmus W.R. (1969). In *Meteorite Research* (ed. P. Millman). Reidel, Dordrecht. 408–491;
- [1.20] Anders E. (1964). *Sp. Sci. Rev.* 3, 583–714;
- [1.21] Mason B. (1966). *GCA* 30, 23–29;
- [1.22] Keil K. (1968). *J. Geophys. Res.* 73, 6945–6976;
- [1.23] Sears D.W. et al. (1982). *GCA* 46, 579–608;
- [1.24] Brearley A.J. & Jones R.H. (1998). In: *Planetary Materials* (ed. J.J. Papike). Min. Soc. America, Rev. Mineralogy No. 36;
- [1.25] Ahrens L.H. et al. (1969). In: *Meteorite Research* (ed. P. Millman). Reidel, Dordrecht. 166–173;
- [1.26] Von Michaelis H. et al. (1969). *EPSL* 5, 387–394;
- [1.27] Mason B. (1971). *Handbook of Elemental Abundances in Meteorites* (ed. B. Mason). Gordon and Breach, New York. 555 pp;
- [1.28] Lodders K. & Fegley B. (1998). *The Planetary Scientist's Companion*. Oxford Univ. Press. 371 pp;
- [1.29] Lodders K. (2003). *Ap. J.* 591, 1220–1247;
- [1.30] Weisberg M.K. et al. (1996). *GCA* 60, 4253–4263;
- [1.31] Dodd R.T. et al. (1967). *GCA* 31, 921–951;
- [1.32] Dodd R.T. (1969). *GCA* 33, 161–203;
- [1.33] Dodd R.T. & Van Schmus W.R. (1965). *J. Geophys. Res.* 70, 3801–3811;
- [1.34] Kusunoki K. (1975). *Mem. Natl. Inst. Pol. Res. Sp. Issue.* 5, 1–8;
- [1.35] Whillans I.M. & Cassidy W.A. (1983). *Science* 222, 55–57;
- [1.36] Bischoff A. & Geiger T. (1995). *Meteoritics* 30, 113–122;
- [1.37] Wasson J.T. (1974). *Meteorites*. Springer-Verlag, Berlin. 316 pp;
- [1.38] Afiattalab F. & Wasson J.T. (1980). *GCA* 44, 431–466;
- [1.39] Huss G.R. et al. (1981). *GCA* 45, 31–51;
- [1.40] Sears D.W. et al. (1980). *Nature* 287, 791–795;
- [1.41] McSween H.Y. Jr. (1979). *Rev. Geophys. Space Phys.* 17, 1059–1078;
- [1.42] Clayton R.N. & Mayeda T.K. (1996). *GCA* 60, 1999–2018;
- [1.43] Clayton R.N. & Mayeda T.K. (1999). *GCA* 63, 2089–2104;
- [1.44] Clayton R.N. et al. (1991). *GCA* 55, 2317–2338;
- [1.45] Clayton R.N. (2007). In: *Meteorites, Comets, and Planets* (ed. A.M. Davis), Vol. 1 *Treatise on Geochemistry* (eds. H.D. Holland & K.K. Turekian), Elsevier-Pergamon, Oxford, Ch. 1.06, 129–142;
- [1.46] Howard E.C. (1802). *Phil. Trans. Roy. Soc. London.* 192, 168–212;
- [1.47] Kallemeyn G.W. et al. (1991). *GCA* 55, 881–892;
- [1.48] Weisberg M.K. et al. (2001). *MAPS* 36, 401–418;
- [1.49] Bischoff A. et al. *GCA* 57, 2631–2648;
- [1.50] Rubin A.E. & Kallemeyn G.W. (1980). *GCA* 53, 3035–3044;
- [1.51] Schulze H. et al. (1994). *Meteoritics* 29, 275–286;
- [1.52] Stöffler D. et al. (1991). *GCA* 55, 3845–3867;
- [1.53] Rubin A.E. et al. (1997). *GCA* 61, 847–858;
- [1.54] Scott E.R.D. et al. (1992). *GCA* 56, 4281–4293;
- [1.55] Wlotzka F. (1993). *Meteoritics* 28, 460;
- [1.56] Mason B. (1967). *Am. Sci.* 55, 429–555;
- [1.57] Burke J.G. (1986). *Cosmic Debris*. Univ. California Press, Berkeley. 445 pp;
- [1.58] Buchwald V.F. (1975). *Handbook of Iron Meteorites I–III*. Univ. California Press, Berkeley. 1418 pp;
- [1.59] Scott E.R.D. & Wasson J.T. (1975). *Rev. Geophys. Space Phys.* 13, 527–546;
- [1.60] Benedix G.K. et al. (1998). *GCA* 62, 2535–2553;
- [1.61] Benedix G.K. et al. (2000). *MAPS* 35, 1127–1141;
- [1.62] MacPherson G.J. (2007). In: *Meteorites, Comets, and Planets* (ed. A.M. Davis), Vol. 1 *Treatise on Geochemistry* (eds. H.D. Holland & K.K. Turekian), Elsevier-Pergamon, Oxford, Ch. 1.08, 201–247;
- [1.63] Gray C.M. et al. (1973). *Icarus* 20, 213–239;
- [1.64] MacPherson G.J. et al. (1988). In: *Meteorites and the Early Solar System* (eds. J.F. Kerridge & M.S. Matthews). Univ. Arizona Press, Tucson, Arizona. 746–807;
- [1.65] Amelin Y. et al. (2002). *Science* 297, 1678–1683;
- [1.66] Wark D.A. & Lovering J.F. (1977). *Proc. 8th Lunar Sci. Conf.* 95–112;
- [1.67] Connelly H.C. (2005). In: *Chondrites and the Protoplanetary Disk* (eds. A.N. Krot, E.R.D. Scott & B. Reipurth). *ASP Conf. Series* 341, 215–224;
- [1.68] Wark (1987). *GCA* 51, 221–242;
- [1.69] McPherson G.J. & Grossman L. (1979). *Meteoritics* 14, 479–480;
- [1.70] Grossman L. (1975). *GCA* 39, 433–454;
- [1.71] McPherson G.J. et al. (1985). *GCA* 49, 2267–2279;
- [1.72] McSween H.Y. (1977). *GCA* 41, 1777–1790;

- [1.73] Komatsu M. et al. (2001). *MAPS* 36, 629–641;
- [1.74] Krot A.N. et al. (2004). *GCA* 68, 1923–1941;
- [1.75] Russell S.S. et al. (2005). In: *Chondrites and the Protoplanetary Disk* (eds. A.N. Krot, E.R.D. Scott & B. Reipurth). *ASP Conf. Series* 341, 317–350;
- [1.76] Wasserburg G.J. et al. (1977). *Geophys. Res. Lett.* 4, 299–302;
- [1.77] Papanastassiou D.A. & Brigham C.A. (1989). *Astrophys. J.* 338, L37–L40;
- [1.78] Boss A.P. (1996). In: *Chondrules and the Protoplanetary Disk* (eds. R.H. Hewins, R.H. Jones & E.R.D. Scott). Cambridge Univ. Press. 257–263;
- [1.79] Shu F.H. et al. (1997). *Science* 277, 1475–1479;
- [1.80] Boss A.P. & Durisen R.H. (2005). In: *Chondrites and the Protoplanetary Disk* (eds. A.N. Krot, E.R.D. Scott & B. Reipurth). *ASP Conf. Series* 341, 821–838;
- [1.81] Ciesla F. (2005). In: *Chondrites and the Protoplanetary Disk* (eds. A.N. Krot, E.R.D. Scott & B. Reipurth). *ASP Conf. Series* 341, 811–820;
- [1.82] Gooding J. & Keil K. (1981). *Meteoritics* 16, 17–43;
- [1.83] McSween H.Y. (1977). *GCA* 44, 477–491;
- [1.84] Scott E.R.D. & Taylor G.J. (1983). *J. Geophys. Res.* 88, B275–B286;
- [1.85] Krot A.N. et al. (2005). *Nature* 436, 989–992;
- [1.86] Scott E.R.D. et al. (1988). In: *Meteorites and the Early Solar System* (eds. J.F. Kerridge & M.S. Matthews). Univ. Arizona Press, Tucson, Arizona. 718–745;
- [1.87] Nittler L. (2003). *EPSL* 209, 259–273;
- [1.88] Zinner E. (1998). *AREPS* 26, 147–188;
- [1.89] Anders E. & Zinner E. (1993). *Meteoritics* 28, 490–514;
- [1.90] Zinner E. (1997). In: *Astrophysical Implications of the Laboratory Study of Presolar Materials* (eds. T.J. Bernatowicz & E. Zinner). AIP, New York, pp. 3–26;
- [1.91] Zinner E. (2007). Presolar grains. In: *Meteorites, Comets, and Planets* (ed. A.M. Davis), Vol. 1 *Treatise on Geochemistry* (eds. H.D. Holland & K.K. Turekian), Elsevier-Pergamon, Oxford, Ch. 1.02, 16–49;
- [1.92] Lewis R.S. et al. (1987). *Nature* 326, 160–162;
- [1.93] Huss G.R. & Lewis R.S. (1995). *GCA* 59, 115–160;
- [1.94] Russell S.S. et al. (1996). *MAPS* 31, 343–355;
- [1.95] Verchovsky A.B. et al. (2006). *Ap. J.* 651, 481–490;
- [1.96] Clayton D.D. (1989). *Ap. J.* 340, 613–619;
- [1.97] Clayton D.D. et al. (1995). *Ap. J.* 447, 894–905;
- [1.98] Gilmour J.D. et al. (2005). *GCA* 69, 4133–4148;
- [1.99] Dai Z.R. et al. (2002). *Nature* 418, 157–159;
- [1.100] Hoppe P. et al. (1996). *Science* 272, 1314–1316;
- [1.101] Zinner E. et al. (1989). *GCA* 53, 3273–3290;
- [1.102] Alexander C.M.O'D. (1993). *GCA* 57, 2869–2888;
- [1.103] Hoppe P. et al. (1994). *Ap. J.* 430, 870–890;
- [1.104] Amari S. et al. (1994). *GCA* 58, 459–470;
- [1.105] Amari S. et al. (2001). *Ap. J.* 551, 1065–1072;
- [1.106] Hoppe P. et al. (1995). *GCA* 59, 4029–4056;
- [1.107] Zinner E. et al. (1995). *Meteoritics* 30, 209–226;
- [1.108] Podosek F.A. (2007). Noble gases. In: *Meteorites, Comets, and Planets* (ed. A.M. Davis), Vol. 1 *Treatise on Geochemistry* (eds. H.D. Holland & K.K. Turekian), Elsevier-Pergamon, Oxford, Ch. 1.14, 381–405;
- [1.109] Wieler R. (2002). In: *Noble Gases in Geochemistry and Cosmochemistry* (eds. D. Porcelli, C.J. Ballentine & R. Wieler). *Rev. Mineral. Geochem.* 47, 125–170;
- [1.110] Heber V.S. et al. (2009). *GCA* 73, 7414–7432;
- [1.111] Busemann H. et al. (2000). *MAPS* 35, 949–973;
- [1.112] Ott U. (2002). In: *Noble Gases in Geochemistry and Cosmochemistry* (eds. D. Porcelli, C.J. Ballentine & R. Wieler). *Rev. Mineral. Geochem.* 47, 71–96;
- [1.113] Göbel R. et al. (1978). *J. Geophys. Res.* 83, 855–867;
- [1.114] Rai V.K. et al. (2003). *GCA* 67, 4435–4456;
- [1.115] Bogard D.D. & Johnson P. (1983). *Science* 221, 651–654;
- [1.116] Markowski A. et al. (2007). *EPSL* 262, 214–229;
- [1.117] McKeegan K. & Davis A.M. (2007). In: *Meteorites, Comets, and Planets* (ed. A.M. Davis), Vol. 1 *Treatise on Geochemistry* (eds. H.D. Holland & K.K. Turekian), Elsevier-Pergamon, Oxford, Ch. 1.16, 431–460;
- [1.118] Wadhwa M. (2007). Long-lived chronometers. In: *Meteorites, Comets, and Planets* (ed. A.M. Davis), Vol. 1 *Treatise on Geochemistry* (eds. H.D. Holland & K.K. Turekian), Elsevier-Pergamon, Oxford, Ch. 1.27, 25 pp;
- [1.119] McPherson G.J. et al. (1995). *Meteoritics* 30, 365–386;
- [1.120] Srinivasan G. et al. (1996). *GCA* 60, 1823–1835;
- [1.121] Lugmair G. and Galer S. (1992). *GCA* 56, 1673–1694;
- [1.122] Russell G.J. et al. (1996). *Science* 273, 757–762;
- [1.123] Lugmair G.W. & Shukolyukov A. (1998). *GCA* 62, 2863–2886;
- [1.124] Lee D.C. & Halliday A.N. (1996). *Science* 274, 1876–1879;
- [1.125] Kleine T. et al. (2005). *GCA* 69, 5805–5818;
- [1.126] Markowski A. et al. (2006). *EPSL* 242, 1–15;
- [1.127] Yin Q. et al. (2002). *Nature* 418, 949–952;
- [1.128] Kleine T. et al. (2002). *Nature* 418, 952–955;
- [1.129] Lee D.C. & Halliday A.N. (1995). *Nature* 378, 771–774;
- [1.130] Lee D.C. & Halliday A.N. (1997). *Nature* 388, 854–857;
- [1.131] Quitté G. et al. (2000). *EPSL* 184, 83–94;
- [1.132] Herzog G.F. (2007). Cosmic-ray exposure ages of meteorites. In: *Meteorites, Comets, and Planets* (ed. A.M. Davis), Vol. 1 *Treatise on Geochemistry* (eds. H.D. Holland & K.K. Turekian), Elsevier-Pergamon, Oxford, Ch. 1.13, 347–380;
- [1.133] Masarik J. & Reedy R.C. (1995). *EPSL* 136, 381–395;
- [1.134] Reedy R.C. (1987). *Proc. 17<sup>th</sup> LPSC Conf. J. Geophys. Res.* 92, E697–702;
- [1.135] Eugster O. (1988). *GCA* 52, 1649–1662;
- [1.136] Bogard D.D. (1995). *Meteoritics* 30, 244–268;
- [1.137] Rubin A.E. & Keil K. (1984). *Meteoritics* 19, 135–143;
- [1.138] Scott E.R.D. & Haack H. (1993). *Meteoritics* 28, 434;
- [1.139] MacPherson G.J. (2005). In: *Chondrites and the Protoplanetary Disk* (eds. A.N. Krot, E.R.D. Scott & B. Reipurth). *ASP Conf.* 225–250.